Journal of Power Sources 198 (2012) 243–250

Contents lists available at SciVerse ScienceDirect

Journal of Power Sources

journal homepage: www.elsevier.com/locate/jpowsour

# Tin-coated graphite electrodes as composite anodes for Li-ion batteries. Effects of tin coatings thickness toward intercalation behavior

F. Nobili[a,*], M. Mancini[a], P.E. Stallworth[b], F. Croce[c], S.G. Greenbaum[b], R. Marassi[a]

[a] Scuola di Scienze e Tecnologie, Sezione Chimica, Università di Camerino, Via S. Agostino 1, I-62032 Camerino (MC), Italy
[b] Dept. of Physics and Astronomy, Hunter College (CUNY), 695 Park Ave., New York, NY 10065, United States
[c] Dipartimento di Scienze del Farmaco, Università 'G. D'Annunzio' Chieti-Pescara, Via dei Vestini 31, I-66100 Chieti (CH), Italy

ARTICLE INFO

*Article history:*
Received 19 August 2011
Received in revised form
21 September 2011
Accepted 25 September 2011
Available online 1 October 2011

*Keywords:*
Graphite composite anodes
Sn coatings
Intercalation mechanism
Charge-transfer kinetics
Electrochemical impedance spectroscopy

ABSTRACT

The electrochemical behavior of graphite anodes, coated by 50–500 Å-thick Sn layers, is discussed in the present paper. Morphology and structure of the modified electrode surfaces are described, and the charge/discharge behavior is evaluated by galvanostatic cycles at temperatures down to −30 °C. The enhanced kinetics of the intercalation/deintercalation process is studied by cyclic voltammetry and electrochemical impedance spectroscopy, focusing on the role played by the Sn coatings in the intercalation/deintercalation mechanism.

The results show that the metal layers modify and stabilize the electrode/electrolyte interphase and that the intercalation process is mediated by reversible Li–Sn alloys formation. Moreover, all the Sn coatings are effective in modifying the energy barriers related both to the $Li^+$ desolvation step and to the migration of the desolvated $Li^+$ ion through the modified surface layers. As a consequence, the overall polarization for the charge-transfer process is reduced, and enhanced low-temperature intercalation performances are obtained.



## 1. Introduction

Since the introduction of Li-ion batteries technology, graphite has been the preferential choice as active material for the negative electrode, due to the stability of the electrode/electrolyte interphase, the low and flat operating voltage, and the high specific capacity [1]. Nevertheless, graphite anode utilization at demanding conditions, such as high charge–discharge rates or very low temperatures (below −20 °C) is hindered by a severe polarization that forces the electrode to approach metal Li deposition potential before the intercalation process is complete, interrupting the battery charge [2–5]. This behavior can be ascribed to ohmic polarization (related to bulk electrode, electrolyte and passivation layer) and to kinetic limitations (involving solid-state diffusivity of $Li^+$ or activation of the charge-transfer process).

In the attempt to overcome these limitations, electrode coating with thin metal or metal oxide layers has been proposed as a versatile surface modification technique [6–14]. It has been demonstrated that physical vapor deposition (PVD) is an inexpensive and simple technique for the coating of graphite anodes with very thin (50 Å) layers of a wide array of metals (Ag, Al, Au, Bi, Cu, In, Ni, Pb, Pd, Sn, Zn) [15]. Among them, Cu- and Sn-coated electrodes have shown the best cycling behavior [16,17], with the only drawback of an increased first cycle irreversible capacity, probably due to the involvement of the metal surface in the solid electrolyte interphase (SEI) formation. Remarkable results have been obtained at the low temperature limit (−30 °C), with reversible capacities up to 30% and 40% of the theoretical value for Cu- and Sn-coated anodes respectively. Recently, Cu or Sn coatings have been applied to other anodic materials as anatase $TiO_2$, confirming an improvement of the electrochemical behavior [18,19].

The origin of improved low-temperature (low-T) intercalation ability of the coated graphite anodes and the mechanism of migration through the interfacial metal coatings are still under investigation. In fact, only some of the layered metals (as Sn) are able to form reversible alloys with Li, actively contributing to the charge exchanged by the electrodes. In addition, even when alloying is possible the contribution to capacity is not relevant because of the very low relative amounts of metals involved. For other metals (as Cu), the formation of intermetallic compounds in the potential windows at which graphite anodes operate is not possible. Nevertheless, also for this class of electrodes the mass transfer of $Li^+$ through surface metal layer is still possible, because of vacant spaces in the metal lattice and phonon-breathing phenomena [20], and the low-T performances are improved as well.

With the aim to explain this behavior, the intercalation kinetics has been investigated revealing, for both Cu- and Sn-coated

* Corresponding author. Tel.: +39 0737 402210; fax: +39 0737 402296.
*E-mail address:* francesco.nobili@unicam.it (F. Nobili).

0378-7753/$ – see front matter © 2011 Elsevier B.V. All rights reserved.
doi:10.1016/j.jpowsour.2011.09.075

electrodes, a dramatic reduction of polarization. This has been attributed to an increase of conductivity of SEI and of bulk electrode and, mainly, to a catalysis toward the charge-transfer process. The catalytic effect has been confirmed by the reduction of the related activation energy, as calculated in the temperature range 20 to −30 °C [17].

Charge-transfer kinetics of electrodes coated by Cu layers of thickness in the range 50–500 Å has been evaluated as well [21]. It has been confirmed that Cu layers can catalyze the charge-transfer process, but at the same time, being not able to form alloys with Li, they can partly hinder $Li^+$ migration, acting as physical barriers, when their thickness is increased.

Several authors have investigated the charge-transfer mechanism at the interphase between graphite electrodes and electrolyte, agreeing that the desolvation of $Li^+$ ions at electrode surface has a strong influence in the related kinetics [22–25]. Very recently, Xu et al. [26] demonstrated that the activation energy for the charge-transfer is made up by two main contributions. One is related to the desolvation of $Li^+$ ions, and can be ascribed to the energy necessary to break up the $Li^+$ ion solvation sheet. The other is an interphase contribution due to $Li^+$ ion migration through SEI toward the intercalation sites.

In this context, in the present paper we evaluate several aspects, related to the Sn coatings, that may affect thermodynamics and kinetics of Li intercalation: (i) the role of Sn layers in modifying electrode/electrolyte interphase; (ii) the action of the Sn layers as physical barriers and the mechanism of $Li^+$ migration through them; (iii) the possible contribution to reversible capacity given by Li–Sn alloys; (iv) the Sn catalytic action toward the charge-transfer process. Charge/discharge behavior is characterized in the temperature range 20 to −30 °C by galvanostatic chronopotentiometry. The intercalation/deintercalation kinetics is investigated by cyclic voltammetry and electrochemical impedance spectroscopy in the same temperature range.

## 2. Experimental

Graphite (Timrex KS-15 by Timcall, specific area 12 $m^2\,g^{-1}$, average particle size 7.7 μm, interlayer distance 3.36 Å) has been vacuum dried overnight at 200 °C and subsequently mildly oxidized by thermal treatment in air at 750 °C for 45 min. The oxidation degree has been roughly estimated by weight loss (about 25–30%) and by oxygen content (about 11%) as determined by elemental analysis (Fisons EA1108CHNSO).

The electrodes were prepared using the 'doctor blade' technique that allows control of the loading. The procedure, detailed elsewhere [17], lead to a layer of graphite electrode containing graphite, binder (poly(vinylidene fluoride), PVDF by Aldrich) and conductive carbon (Super-P by MMM Carbon) in the mass ratio 85:10:5, with a loading of about 3 mg $cm^{-2}$. Six different portions were cut from the graphite electrode. One of them was left uncoated and used as a term of comparison for the results (anode A), while the other portions (anodes B–F) were coated with Sn layers of different thicknesses prepared by physical vapor deposition. Suitable currents were applied to a tungsten crucible holding pure Sn metal, in order to evaporate the metal onto the graphite substrates, kept at room temperature. The growth of the coatings has been monitored with a quartz crystal microbalance, resulting in Sn deposits of thicknesses of 50, 100, 150, 250, 500 Å for electrodes B, C, D, E, F respectively.

Electrodes morphology was investigated using a Cambridge Stereoscan mod. 360 scanning electron microscopy (SEM), equipped with detectors for secondary electrons (SE), backscattered electrons (BSE) and X-rays (electron probe micro analysis, EPMA).

All the electrochemical measurements were performed by using T-shaped polypropylene Swagelok-type 3-electrode cells, equipped with stainless steel (SS304) rods as current collectors. Two polypropylene films (Celgard 2300, Celanese Co.) were used as separators. The electrolyte was 1 M $LiPF_6$ in ternary EC:DEC:DMC 1:1:1 (LP71 by Merck). The ternary electrolyte system has been used in order to allow low-temperature measurements without any complications due to solvent freezing [27,28]. High purity Li (Aldrich) was used to prepare counter and reference electrodes. The cells were assembled in an Ar-filled glove box, with $O_2$ and $H_2O$ contents below 10 ppm, cycled 3 times at C/3 rate in order to allow a complete and homogeneous SEI formation, and then opened to evacuate any possible gases developed during the formation of passivation layer. The cells were finally sealed and brought out of the box to complete the electrochemical investigation in a programmable freezer able to control the temperature within ±1 °C.

The electrochemical measurements have been performed by using a VMP2/Z multi-channel electrochemical workstation (Bio-Logic, France). The cells were cycled between 0.01 and 1.5 V at C/5 rate at six different temperatures in the range 20 to −30 °C. Cyclic voltammetries were performed at a very slow scan rate (10 μV $s^{-1}$) at 20 °C in the potential range 0.01–0.3 V. Impedance measurements were acquired at temperatures between 20 and −30 °C in the frequency range 3 mHz to 100 kHz, by superimposing a sinusoidal perturbation of ±5 mV over the bias potential of 0.09 V. All the potentials are given *vs.* $Li^+$/Li redox couple. For sake of comparison, all the values of current, capacity and impedance have been normalized to the active masses of the electrodes.

*Ex situ* $^{19}F$ solid-state magic-angle-spinning nuclear magnetic resonance (MAS-NMR), performed on powders scraped from cycled anodes A and B, was carried out on a Varian Direct Digital Drive spectrometer operating at a field strength of 7.1 T. Spectra were gathered at room temperature from 1000 to 2000 signal averaged transients (with a spinning rate of 22 kHz, single-pulse $\pi/2$ excitation pulse width of 1.6 μs along with a minimum of 15 s recycle delay between transients to prevent sample saturation). Aqueous $Li^+C^{19}F_3SO_3^-$ was used as a reference ($\delta = 0$), as this resonance occurs −78.5 ppm from $CCl_3{}^{19}F$.

## 3. Results and discussion

### 3.1. Morphological and chemical characterization of electrode surface

Scanning electron microscopy was used to investigate topography and composition of electrodes. Fig. 1a–e shows the SE micrographs obtained with electrodes respectively coated by 0, 50, 100, 150, 250 Å (electrodes A, B, C, D, E) of Sn. All the electrodes appear made by uniform dispersions of graphite flakes of micrometer size. No inhomogeneities of Sn coatings are evidenced. On the contrary, the SE micrograph of electrode F (Fig. 1f) reveals a rough structure of the surface that, as confirmed by BSE micrograph in Fig. 1g, can be attributed to some dendritic accumulation of Sn, probably formed because of the relatively high thickness of the metal layer.

Fig. 1h shows the results of electron probe microanalysis averaged on the whole area scanned by the electron beam. The peaks related to $L_{\alpha 1}$ and $L_{\beta 1}$ emission lines of Sn (4.5 keV) have been taken into account, giving a calibration line in which the integrated signals are reported as a function of Sn coatings thickness. Apart a constant bias due to *bremsstrahlung* radiation, and random errors due to the relatively poor counting statistics (acquisition time was 100 s per spectrum), the values can be interpolated by a straight

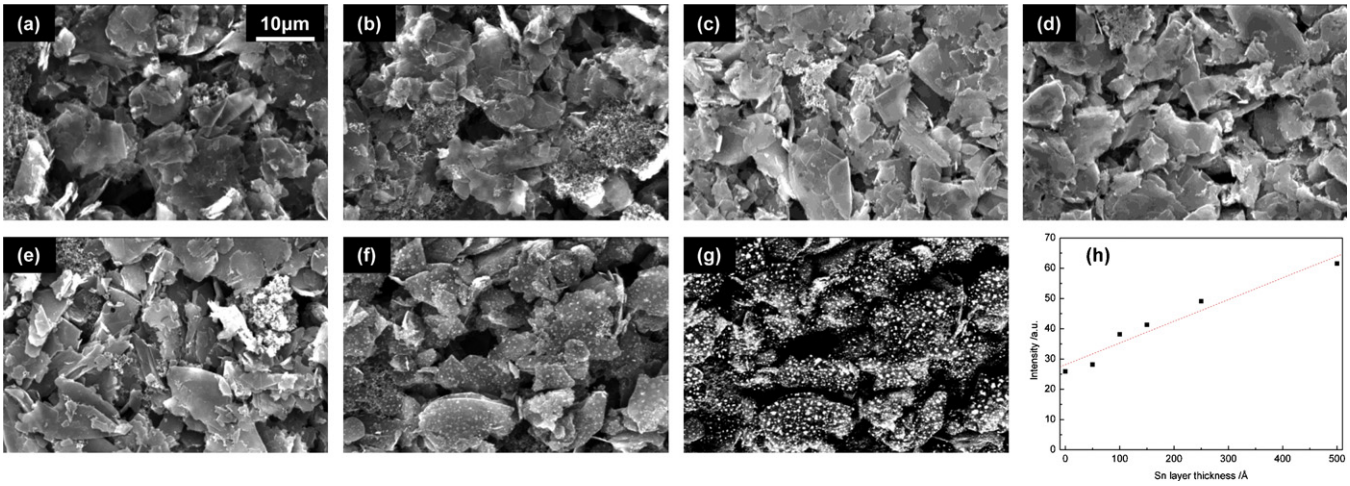


**Fig. 1.** (a–f) Secondary electrons micrographs of electrodes A–F coated by Sn layers of different thicknesses (0, 50, 100, 150, 250, 500 Å). (g) Backscattered electrons image of electrode F. (h) Areas of convolutions of Sn–$L_{\alpha 2}$ and Sn–$L_{\beta 1}$ X-ray peaks (~4.5 keV).

line, confirming the effectiveness and the reliability of the PVD process.

$^{19}$F MAS-NMR was used in order to gain insight into the impact of Sn coatings on passivation layer chemistry. For both anodes, the main signal as seen in Fig. 2 at $\delta = 4.3$ ppm is due to the overlapping of resonances from $PF_6^-$ anion and PVDF binder, while a background signal from polytetrafluoroethylene (PTFE) in the NMR probe is located near −50 ppm. Also observed for the uncoated electrode A is a small signal located near −125 ppm. This feature has been observed in studies of Li/$CF_x$ primary cells and is attributed to the irreversible formation of LiF on discharge [29]. In the present case, the presence of LiF is indicative of $LiPF_6$ decomposition, a process usually accelerated by water [30]. The fact that the LiF feature is not evident in the case of the 50 Å Sn-coated electrode B (while present for electrode A) suggests that the Sn coating may be effective in preventing $LiPF_6$ decomposition, caused by moisture traces eventually contained at ppm level in the solvent and/or in the glove-box atmosphere.

### 3.2. Charge/discharge behavior

Cycle life of anodes A–F has been evaluated, at a temperature of 20 °C, by galvanostatic cyclations performed at C/5 charge/discharge rate, in the potential range 0.01–1.5 V. In Fig. 3 the reversible capacity values are reported. All the electrodes exhibit stable capacities over 40 cycles. For all the anodes the reversible capacities are close to the graphite theoretical value of 372 mAh $g^{-1}$, with only slightly lower values (about 340–350 mAh $g^{-1}$) for the electrodes E and F, coated by the thickest Sn layers (250 and 500 Å respectively). These values, detailed in Table 1, suggest that when thicker metal coatings are applied over the electrode surface, the interphase can partly act as a mechanical barrier against Li intercalation and deintercalation [26]. The kinetic aspects related to this behavior are detailed in the following of the paper.

Table 1 also evidences that the first cycle irreversible capacity increases when the anodes are coated by Sn. This behavior can be ascribed to two main causes. First, a possible irreversible reaction between $Li^+$ and surface tin oxides SnO or $SnO_2$, that could have been formed either because of the exposure to the air of the electrodes during their fabrication or by reaction of the Sn layer with

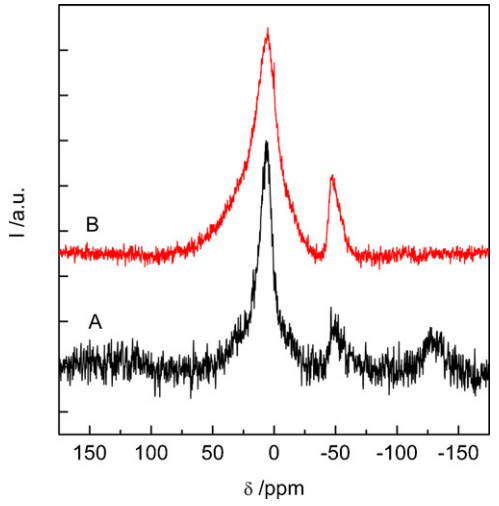


**Fig. 2.** *Ex situ* NMR spectra of un-coated (A) and 50 Å Sn-coated (B) anodes. Reference line = $Li^+CF_3SO_3^-$ resonance line @ −78.5 ppm from $CCl_3F$.

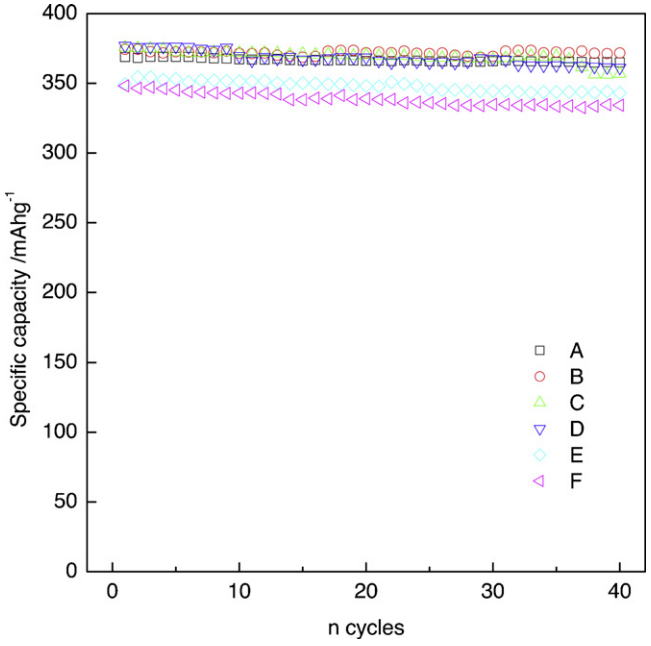


**Fig. 3.** Reversible capacity of electrodes A–F. $T = 20$ °C, $0.01 < E < 1.5$ V, and charge/discharge rate = C/5.

**Table 1**
Summary of irreversible and reversible specific capacities (mAh g$^{-1}$) for electrodes A–F. $T$ = 20 °C.

| Electrode | Sn layer thickness/Å | 1st cycle irrev. capacity at C/3 | Reversible capacity at C/5 | Li–Sn theoretical capacity[a] |
|---|---|---|---|---|
| A | 0 | 84 | 367 | 0 |
| B | 50 | 135 | 371 | 1 |
| C | 100 | 139 | 369 | 2 |
| D | 150 | 113 | 368 | 4 |
| E | 250 | 153 | 348 | 6 |
| F | 500 | 140 | 339 | 12 |

[a]The theoretical contributions of Li–Sn alloying to the capacity of the electrodes have been calculated by taking into account $Li_{22}Sn_5$ formation and are normalized to the overall mass of the active materials (graphite and Sn) of the electrodes (loading = 3 mg cm$^{-2}$).

the traces of moisture contained in the electrolyte. Second, the formation of a modified passivation layer that may also involve the Sn metal in contact with the electrolyte.

The amounts of metal that cover the electrodes are very low, with mass ratios Sn:graphite in the range 0.12–1.2%, as calculated taking into account the loading of graphite (3 mg cm$^{-2}$) and the thicknesses of the Sn layers (0–500 Å). As a consequence, the theoretical contribution of Li–Sn alloying to the charge exchanged by the electrodes is never relevant, as evidenced in Table 1. The actual contribution of Sn to reversible and irreversible processes can be evaluated by the differential analysis of the intercalation profiles of the electrodes coated by thicker metal layers. Fig. 4 shows the *dQ*/*dE* differential profiles, at different magnification levels, corresponding to selected galvanostatic cycles of electrode F, coated by a 500 Å Sn layer.

Two peaks related to irreversible processes can be identified at about 1 V and 0.75 V during the first intercalation. They correspond, respectively, to the irreversible reaction of $Li^+$ with tin oxides SnO or $SnO_2$ [31] and to the formation of the solid electrolyte interphase (SEI) over the electrode surface. The SEI formation process extends to lower potentials contributing to a relevant background down to 0.25 V. Below this potential, the peaks related to the formation of Li-graphite intercalation compounds (GICs) are the only features evidenced. The subsequent cycles are only characterized by reversible peaks which can be ascribed to the Li intercalation into graphite, the main processes in the range 0.25–0.01 V [32], and to Li–Sn reversible alloying occurring at voltages below 0.75 V [31,33,34]. This demonstrates that reversible intermediates, related

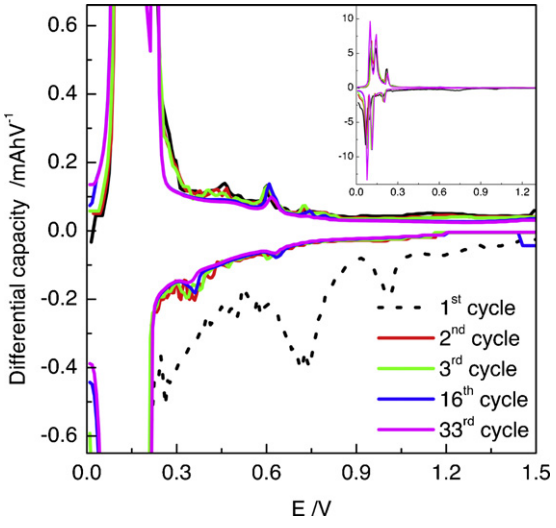


**Fig. 4.** *dQ*/*dE* differential plots of selected galvanostatic cycles of electrode F. $T$ = 20 °C. Charge/discharge rates = C/3 for cycles 1–3, C/5 for cycles 16, 33.

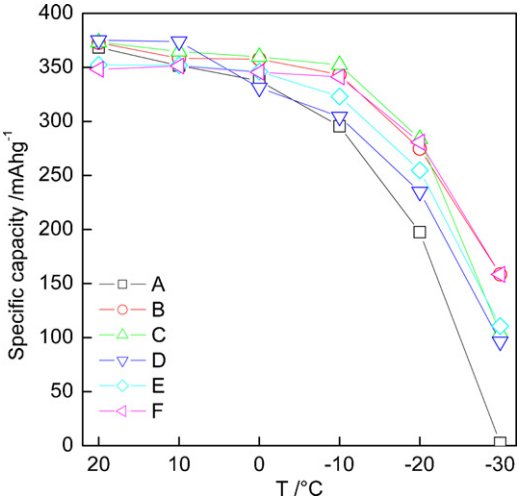


**Fig. 5.** Specific capacity as a function of temperature and Sn layer thickness. Charge/discharge rate = C/5, 0.01 < $E$ < 1.5 V.

with inter-metallic Li–Sn reactions, are formed at the electrode surface.

These findings evidence a major differentiation with the intercalation behavior already observed for Cu-coated graphite anodes [20], where $Li^+$ migration is allowed only by phonon-breathing phenomena and lattice vacancies. In the present case, the migration of $Li^+$ through Sn layers and the subsequent GICs formation can be described as an alloy-mediated intercalation. After $Li^+$ desolvation and adsorption at electrode surface [17,22–26], Li–Sn alloys start to reversibly form at electrolyte/Sn interphase, forming a moving-boundary that reaches Sn/graphite interphase, where lithium is transferred to the graphite intercalation sites.

In addition, the reversibility of the processes upon cycling reveals that, at least under the experimental conditions here adopted, the Sn layers are mechanically stable. This behavior can be tentatively explained with the low thicknesses of the Sn coatings (5–50 nm). It may be hypothesized that metal layers at this level of thickness are able to accommodate the large relative volume variations usually associated with Li–Sn alloying/dealloying processes [34–36].

Fig. 5 shows the trends of the reversible capacity of the electrodes in the temperature range between 20 and −30 °C. At each temperature the capacity has been calculated as the average value of five subsequent cycles, performed at C/5 charge/discharge rate between 0.01 and 1.5 V. In the temperature range 20–0 °C the capacity values are comparable for all the electrodes, but when the temperature is progressively lowered to −10, −20, −30 °C some differentiations arise. The most relevant result is that the uncoated electrode always exhibits the worst behavior, with capacities of 200 mAh g$^{-1}$ at −20 °C and about 0 mAh g$^{-1}$ at −30 °C. On the contrary, all the coated electrodes show reversible capacities between 250 and 300 mAh g$^{-1}$ at −20 °C and between 100 and 150 mAh g$^{-1}$ at −30 °C. Such high values, as already evidenced in Fig. 4, cannot be attributed to extra contributions of Li–Sn alloys to reversible capacity, but rather to an effect of the metal layers in reducing the overall electrode polarization, that allows to accommodate higher amounts of Li before the cut-off potential (10 mV) is approached. These results confirm our previous findings that showed higher low-temperature capacities for metal–graphite composite electrodes. We explained this behavior claiming two main processes, both related to the presence of the metal layers. Namely, (i) a reduction of the ohmic polarization caused by the SEI and the bulk electrode and (ii) a beneficial catalytic effect on the

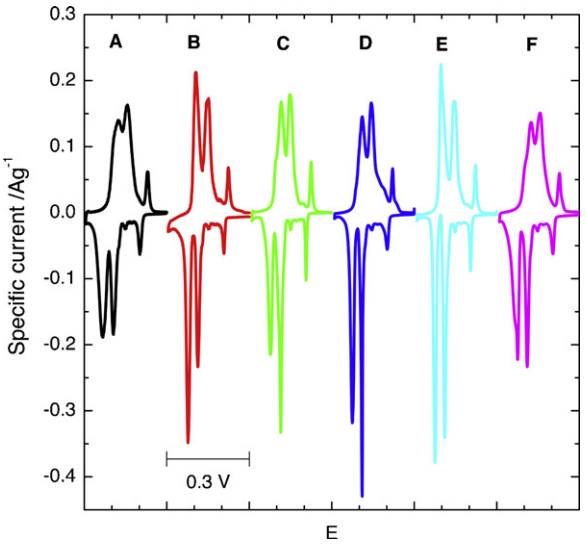


**Fig. 6.** Cyclic voltammograms of electrodes A–F. $T = 20\,^{\circ}C$ and scan rate = 10 μV s$^{-1}$. The voltammograms are shifted along $E$ axis for sake of comparison.

charge-transfer process regarding, specifically, the lithium-ion desolvation step [15–17,21].

### 3.3. Cyclic voltammetry

In order to gain insight into the effects of Sn layers toward intercalation/deintercalation kinetics of the anodes, cyclic voltammetry (CV) has been performed in the potential range 0.01–0.3 V at very slow scan rate (10 μV s$^{-1}$). Fig. 6 shows the voltammetric profiles of electrodes A–F. The mean values ($Ep_{mean}$ in Table 2) of the intercalation and deintercalation peak potentials, related to the three main processes, are comparable for all the electrodes, and scattered of only few mV around the typical equilibrium potentials for $LiC_6/LiC_{12}$, $LiC_{12}/LiC_{27}$, $LiC_{36}/LiC_{72}$ systems. This confirms that the metal coatings have no impact on thermodynamics of Li-graphite intercalation compounds (GICs) formation. When the shape of the voltammograms is taken into account, all the coated electrodes exhibit sharper and higher peaks than the uncoated one, which can be regarded as a signature of faster intercalation/deintercalation kinetics. This is confirmed by the analysis of the separations between the anodic and cathodic potentials of the three GICs formation processes ($\Delta E = Ep_{an} - Ep_{cath}$ in Table 2). $\Delta E$ values are strongly reduced when the coatings are applied. For $LiC_{36}/LiC_{72}$ equilibrium $\Delta E$ corresponds to 28 mV for un-coated electrode, while it never exceeds 20 mV for the coated ones. For the $LiC_{12}/LiC_{27}$ and $LiC_6/LiC_{12}$ equilibria the kinetics improvements are even more marked, since the $\Delta E$ values are respectively of 51 and 58 mV for the un-coated electrode, while they never exceed 45 and 48 mV for the coated anodes. Among the coated anodes, the largest $\Delta E$ is consistently found for the 500 Å Sn-coated anode. This

**Table 2**
Mean values ($Ep_{mean}$) and distances ($\Delta E$) between anodic and cathodic potentials (mV) of the main CV peaks for electrodes A–F.

| Electrode | $LiC_6/LiC_{12}$ | | $LiC_{12}/LiC_{27}$ | | $LiC_{36}/LiC_{72}$ | |
|---|---|---|---|---|---|---|
| | $Ep_{mean}$ | $\Delta E$ | $Ep_{mean}$ | $\Delta E$ | $Ep_{mean}$ | $\Delta E$ |
| A | 95 | 58 | 130 | 51 | 216 | 28 |
| B | 91 | 28 | 131 | 35 | 216 | 15 |
| C | 96 | 38 | 131 | 31 | 216 | 20 |
| D | 93 | 36 | 128 | 33 | 207 | 10 |
| E | 86 | 22 | 128 | 35 | 214 | 16 |
| F | 100 | 48 | 134 | 45 | 219 | 20 |

suggests that, at higher thickness values, the reduction in polarization, induced by the catalytic effect of metal layer toward the $Li^+$ ion desolvation, may be partly balanced by a reduced mobility of $Li^+$ ion through thicker metal layers, that represent the interphase between electrolyte and active graphite. The observed behavior is in agreement with the findings by Abe [24,25] and Xu [22,23,26,37]. These authors demonstrated that the charge-transfer kinetics is bound to the chemistry of electrolyte and SEI, and that the activation energy of the process is made up by two main contributions related to two subsequent steps: (i) the complete desolvation of the $Li^+$ ion adsorbed at the electrode surface (in accordance with the 'adatom' model by Bruce and Saïdi [38]) and (ii) the migration through the interphase. In the cited papers, an interphase made only of electrolyte decomposition products (SEI) was considered, and the effects of the electrolyte composition onto both passivation layer chemistry and $Li^+$ ion desolvation rate were taken into account [23,26]. In the present case, the Sn layers are involved in the surface layer, so that their impact toward the rates of desolvation and migration through the modified electrode/electrolyte interphase has to be considered.

### 3.4. Electrochemical impedance spectroscopy

Electrochemical impedance spectroscopy has been performed at various temperatures ranging from 20 to −30 °C, in the attempt to evaluate the different contributions of the Sn coatings to the intercalation/deintercalation kinetics. The impedance dispersions have been acquired in the frequency range 3 mHz to 100 kHz at 0.09 V, corresponding to the equilibrium potential between $LiC_6$ and $LiC_{12}$ phases.

Fig. 7a–f shows the impedance dispersions of all the electrodes under examination at three relevant temperatures: 20 °C (panels a for electrode A and B and b for electrodes C–F), 0 °C (panels c and d), and −30 °C (panels e and f). Similar dispersions have been obtained at the other investigated temperatures and are not shown here for sake of brevity. Some features are common to the Nyquist plots of every electrodes: (i) a line at low frequencies related to the diffusion toward a blocking electrode, with a more or less pronounced inflection that describes $Li^+$ ion diffusion through heterogeneous media (*i.e.* graphite, metal layers, solid electrolyte, liquid electrolyte in the graphite pores) [15,39,40]; (ii) a semicircle at medium frequencies related to the interfacial charge-transfer and to the formation of the electrical double layer; (iii) an arc at high frequencies related to the accumulation of charge at the surface and conduction through the SEI; (iv) an intercept with the real axis related to the resistance of the electrolyte. The electrolyte contribution, of few Ohms for all the electrodes, has been subtracted from the shown Nyquist plots in order to ease the comparison between the other features.

All the dispersions have been fitted to an equivalent circuit already used to model the data obtained with several metal–graphite composite anodes [15–17,21]. The circuit may be written, by using the Boukamp's notation [41], as $R_{el}(R_{SEI}C_{SEI})(R_{ct}C_{dl})W$, where $R_{el}$, $R_{SEI}$ and $R_{ct}$ represent the resistances respectively associated with electrolyte, passivation layer and charge-transfer process, $C_{SEI}$ and $C_{dl}$ describe the capacitances of passivation layer and double layer, $W$ is the Warburg impedance due to diffusion. In the fitting procedure, all $C$ and $W$ elements have been substituted with constant phase elements $Q$ in order to take into account any deviations from ideal behavior, due to inhomogeneities and roughness in composition and morphology of electrodes and passivation layers [42]. The $\chi^2$ values obtained were in all cases of the order of $10^{-5}$, confirming the reliability of the model.

Fig. 8 shows the values of the passivation layer resistance $R_{SEI}$ at various temperatures. Since the medium-frequency semicircles tends to partly overlap with the high-frequency arcs related to the

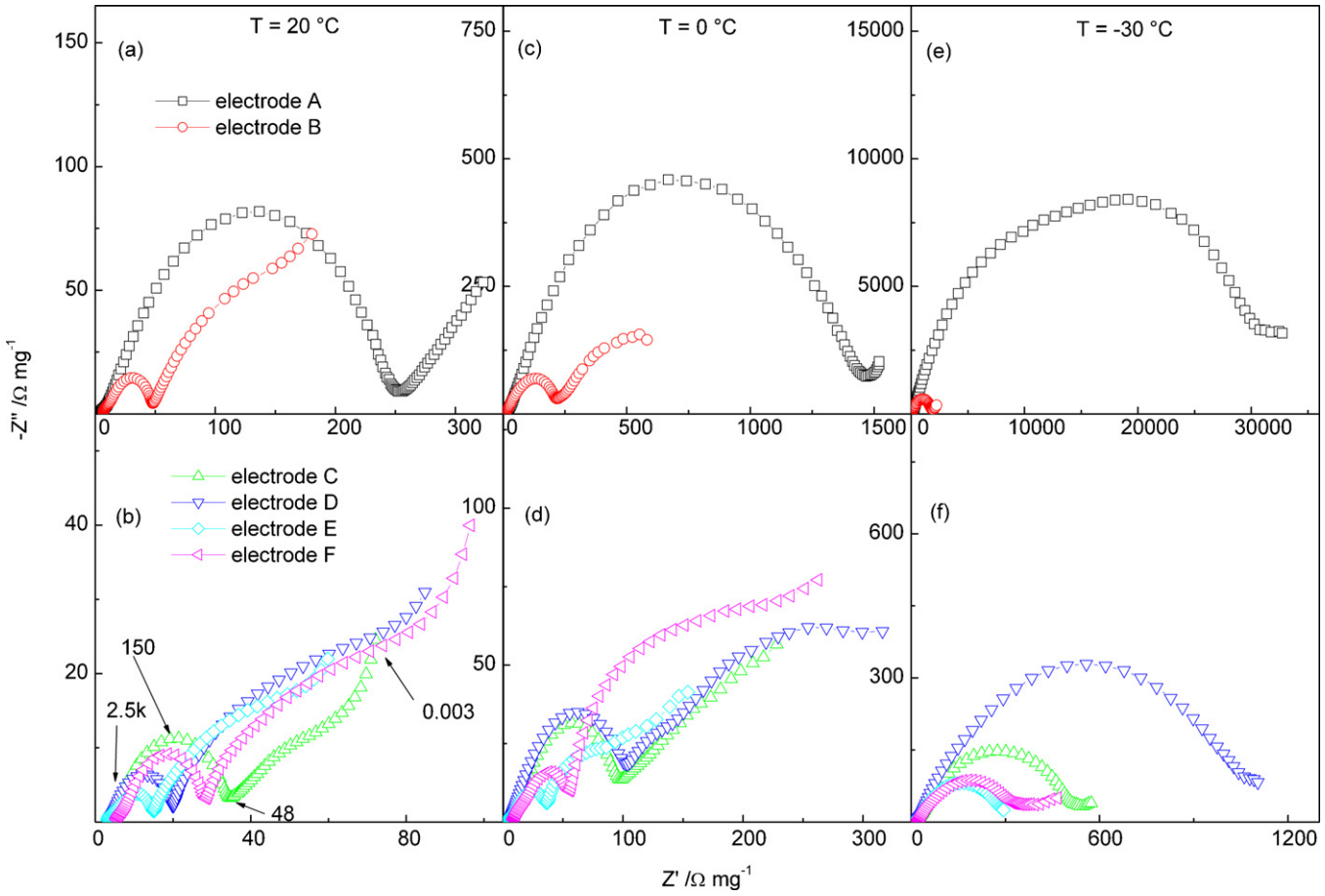


**Fig. 7.** Nyquist plots recorded at 20, 0, −30 °C for electrodes A and B (panels a, c, e) and C–F (panels b, d, f). $E = 0.09$ V, $0.003 < f < 100{,}000$ Hz. Some characteristic frequencies are shown in panel (b) for electrode C (-△-), coated by a 100-Å Sn layer.

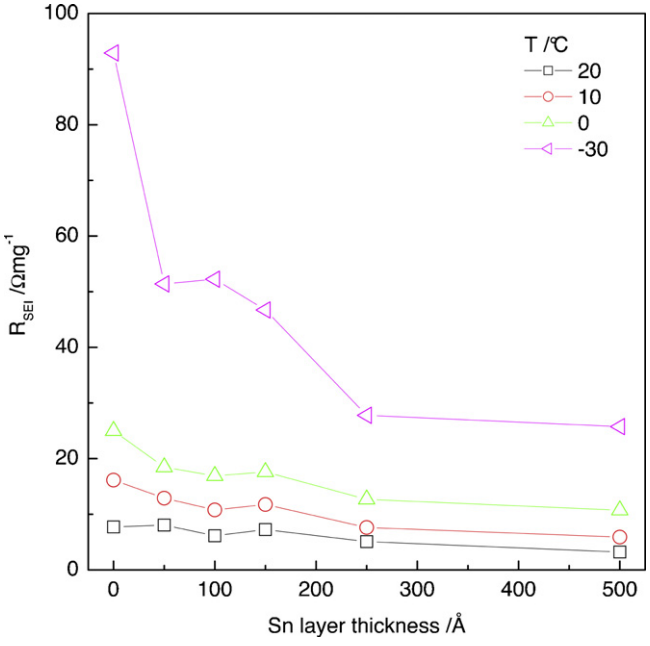


**Fig. 8.** Values of SEI resistances at selected temperatures as a function of the thickness of the Sn layers coating the electrodes A–F. $E = 90$ mV.

SEI, the fitting procedure may lead, especially at low temperatures, to results that are affected by some bias. However, at every temperatures a reduction of the SEI resistance, as the thickness of Sn coatings is increased, can be observed. By taking in account second Ohm's law $R = \rho^* l/S$, the Sn coatings may affect all the three parameters that contribute to the overall resistance. Since it has been supposed that Sn takes directly part in the formation of a modified passivation layer, it may be expected that thicker Sn coatings lead to higher values for the overall SEI thickness $l$. As a consequence, a reduction in $\rho$ and/or an increase in $S$ must be invoked to explain the $R_{SEI}$ reduction exhibited by thicker Sn coatings. Both $\rho$ reduction and $S$ increase are consistent with the composition and morphology of the anodes under investigation. In fact, the incorporation of the metal coating in a passivation layer otherwise made of fluorides, polymers and LiOC-compounds [43] may lead to a decrease in its specific resistivity $\rho$. On the other hand, Sn coatings may induce modifications of the morphology of the interphase, with a possible modification of the surface area $S$. The higher irreversible capacities (Table 1) and the rough morphologies, evidenced in the SEM micrographs by all the Sn-coated anodes (Fig. 1a–e) and especially by electrode F (Fig. 1f and g), are compatible with an increased area of the electrode/electrolyte interphase.

Fig. 9 shows the $R_{ct}$ values as function of Sn coating thickness. At all the temperatures, the un-coated anode A exhibits the largest charge-transfer resistance. For all the coated anodes B–F the values are about one order of magnitude lower. The kinetics of the charge-transfer process is improved because of the higher electronic density conferred to the surface by the Sn coatings. This

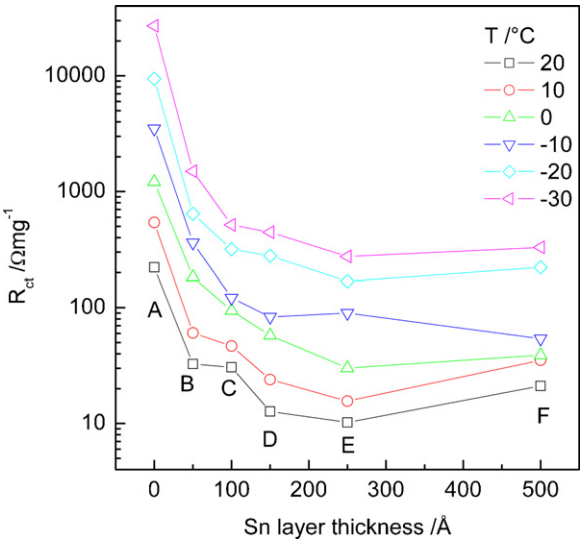


**Fig. 9.** Values of charge-transfer resistances as a function of the temperature and of the thickness of the Sn layers coating the electrodes A–F. $E$ = 90 mV.

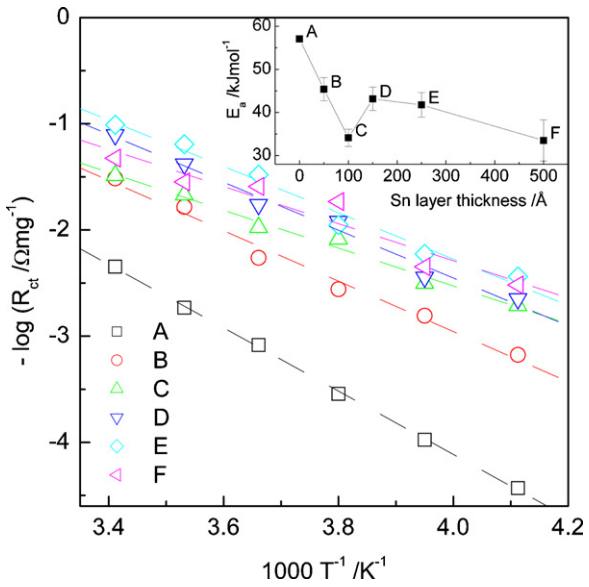


**Fig. 10.** Arrhenius plots related to exchange current density (~1/$R_{ct}$). The calculated activation energy values are shown in the inset.

enhances nucleophilicity of electrode surface and catalyzes the complete removal of solvation atmosphere from intercalating $Li^+$ ions [15–17].

Nevertheless, as was the case for Cu-coated graphite anodes [21], at any temperature the graph $R_{ct}$ *vs.* coating thickness exhibits a non-monotonous behavior, with maxima and/or minima. This confirms that two different trends tend to overlap when the thickness of metal coatings is increased. First, the desolvation of $Li^+$ ions is enhanced by higher amounts of Sn, as the electronic density, that catalyzes the process, is enriched and at the same time the area of the active electrode surface is increased (as confirmed by the roughness of the surface, by the increase in irreversible capacity and by the reduction in $R_{SEI}$). On the other hand, the migration through the surface layer is partly hindered, since the $Li^+$ ion must travel a longer path through Sn interphase before reaching graphite intercalation sites. The final result is that, apart minor experimental deviations, at all the temperatures the charge-transfer resistance is reduced when the Sn layer thickness is increased up to 250 Å, while for 500 Å coatings a slight increase of $R_{ct}$ is generally observed.

Taking into account the activation energies related to interfacial charge-transfer can validate the hypothesis of this dual role of Sn layers. Since charge-transfer is an activated process, the dependence of $R_{ct}$, and of exchange current density $i_0 \sim 1/R_{ct}$, on temperature $T$ can be described in terms of Arrhenius plots of the type $1/R_{ct} = A\exp(-E_a/RT)$, where $A$, $E_a$ and $R$ represent, respectively, a pre-exponential factor, the activation energy for the charge-transfer and the universal constant of gases. The Arrhenius plots for electrodes A–F and the corresponding $E_a$ values are shown in Fig. 10.

As for $R_{ct}$, a non-monotonous trend of $E_a$ *vs.* layer thickness is observed in the inset. This confirms that two main contributions build up in determining the overall 'ion transfer barrier' [26], *i.e.* the one related to the desolvation of the $Li^+$ adsorbed ion and the one determined by the migration through the interphase between active graphite sites and electrolyte. For both contributions, the values depend on interphase chemistry, that is in turn determined by the chemistry of electrolyte and of anode surface. In the cited paper [26], Xu et al. calculated the energy barrier due to $Li^+$ ion desolvation as a baseline value around 50 kJ mol$^{-1}$, and the barrier due to the migration through the interphase as an extra contribution of about 10–20 kJ mol$^{-1}$, depending on electrolyte composition.

In the present case, the interphase between electrolyte and intercalating graphite is modified by the Sn coating, that has a catalytic role and takes part both in SEI and in Li–Sn intermetallic compounds formation. The un-coated electrode exhibits an activation energy of about 57 kJ mol$^{-1}$. This value is comparable with the values reported by Xu et al. [26] and may be considered in the present case as a reference value for graphite anodes, containing contributions only from $Li^+$ desolvation and migration through a 'classical' SEI. When Sn layers cover graphite, they affect both contributions to the overall energy barrier for intercalation. In fact, desolvation of the adsorbed $Li^+$ ion is catalyzed at electrode surface (as already demonstrated for other graphite/metal composite anodes in Refs. [15–17,21]). As the amount of Sn is increased, the area and the electronic density of the catalytic surface are increased as well, and the 'desolvation contribution' to the activation energy is reduced. At the same time, thicker Sn layers, other than modifying the resistivity of the interphase (Fig. 7), tend to increase the length of the migration path. This affects the 'interphase contribution' to the activation energy, with the final result that the overall energy barrier exhibit the non-monotonous behavior reported in Fig. 9b. Up to 100 Å (electrodes B and C), the desolvation and the interphase contributions act in the same direction, both reducing the overall activation energy to around 35 kJ mol$^{-1}$. When the thickness is further increased up to 250 Å (electrodes D and E), the value is slightly increased to values about 45 kJ mol$^{-1}$, confirming that desolvation and interphase contributions tend to balance themselves. Finally, for the 500 Å Sn-coated electrode the overall energy barrier is further reduced, probably because at these high Sn levels the inhomogeneous distribution of the metal coating (revealed by SEM, Fig. 1f and g) produces a rougher surface, with higher catalytic activity toward desolvation, while at the same time the inhomogeneous thickness of the layer does not hinder too much the migration through the interphase. The widening of the error bars confirms that the electrode surface tends to become less homogeneous, and consequently the kinetics less predictable, when the thickness of Sn coatings is increased.

Finally, it is worth noting that the activation energy values calculated for Sn-coated anodes are generally lower than those observed for Cu-coated anodes [21]. This is due to the different lithium migration mechanisms involved. In fact, $Li^+$ can cross Cu layers only by exploiting lattice vacancies or vibrations. As a consequence, the energy barrier due to the lithium migration through the metal

interphase is higher for Cu than for Sn coatings, where reversible Li–Sn alloying processes assist the migration.

## 4. Conclusions

The relatively easy and cheap technique of physical vapor deposition allowed the preparation of Sn/graphite composite anodes that deliver, at very low temperatures, much better intercalation performances than un-modified graphite.

The characterization of thermodynamics and kinetics of the intercalation process revealed that Li transport through the Sn interphase is assisted by local Li–Sn alloying/dealloying processes, that however do not significantly contribute to reversible capacity. The increase of performances has been explained as a combination of several effects due to the Sn layers. In fact, the metal coatings are effective both in preventing electrolyte decomposition by moisture traces and, mainly, in enhancing intercalation kinetics of $Li^+$ ion. The electrochemical impedance spectroscopy revealed that the Sn coatings affect the energy barrier contributions related both to the desolvation step and to the migration through electrode/electrolyte interphase. This dual action allowed to explain the dependence of charge-transfer resistance, and of the related activation energy, on Sn coatings thickness.

## Acknowledgement

The portion of the work done at Hunter College was supported by the U.S. Department of Energy, Grant number DE-SC0005029.

## References

[1] M.B. Armand, in: D.W. Murphy, J. Broadhead, B.C. Steele (Eds.), Material for Advanced Batteries, Plenum Press, New York, 1980, p. 145.
[2] C.K. Huang, J.S. Sakamoto, J. Wolfenstine, S. Surampudi, J. Electrochem. Soc. 147 (2000) 2893.
[3] S.S. Zhang, K. Xu, T.R. Jow, Electrochim. Acta 48 (2002) 241.
[4] H.P. Lin, D. Chua, M. Salomon, H.C. Shiao, M. Hendrickson, E. Plitcha, S. Slane, Electrochem. Solid-State Lett. 4 (2001) A71.
[5] G. Nagasubramanian, J. Appl. Electrochem. 31 (2001) 99.
[6] T. Takamura, J. Suzuki, C. Yamada, K. Sumiya, K. Sekine, Surf. Eng. 15 (1999) 225.
[7] B. Veeraraghavan, A. Durairajan, B. Haran, B. Popov, R. Guidotti, J. Electrochem. Soc. 149 (2002) A675.
[8] T. Takamura, K. Sumiya, J. Suzuki, C. Yamada, K. Sekine, J. Power Sources 81 (1999) 368.
[9] H. Momose, H. Hombo, S. Takeuchi, T. Horiba, M. Oda, M. Koseki, Y. Muranka, Y. Kozono, J. Power Sources 68 (1997) 208.
[10] K. Nishimura, H. Honbo, S. Takeuchi, T. Horiba, M. Oda, M. Koseki, Y. Muranaka, Y. Kozono, H. Miyadaera, J. Power Sources 68 (1997) 436.
[11] S. Kim, Y. Kadoma, H. Ikuta, Y. Uchimoto, M. Wakihara, Electrochem. Solid State Lett. 4 (2001) A109.
[12] J. Gao, H.P. Zhang, L.J. Fu, T. Zhang, Y.P. Wu, T. Takamura, H.Q. Wu, R. Holze, Electrochim. Acta 52 (2007) 5417.
[13] J. Gao, L.J. Fu, H.P. Zhang, T. Zhang, Y.P. Wu, H.Q. Wu, Electrochem. Commun. 8 (2006) 1726.
[14] I. Sandu, T. Brousse, D.M. Schleich, Ionics 9 (2003) 329.
[15] F. Nobili, S. Dsoke, M. Mancini, R. Tossici, R. Marassi, J. Power Sources 180 (2008) 845.
[16] M. Mancini, F. Nobili, S. Dsoke, F. D'Amico, R. Tossici, F. Croce, R. Marassi, J. Power Sources 190 (2009) 141.
[17] F. Nobili, M. Mancini, S. Dsoke, R. Tossici, R. Marassi, J. Power Sources 195 (2010) 7090.
[18] M. Mancini, P. Kubiak, J. Geserick, R. Marassi, N. Hüsing, M. Wohlfart-Mehrens, J. Power Sources 189 (2009) 585.
[19] M. Mancini, P. Kubiak, M. Wohlfart-Mehrens, R. Marassi, J. Electrochem. Soc. 157 (2010) A164.
[20] J. Suzuki, M. Yoshida, C. Nakahara, K. Sekine, M. Kikuchi, T. Takamura, Electrochem. Solid State Lett. 4 (2001) A1.
[21] F. Nobili, S. Dsoke, M. Mancini, R. Marassi, Fuel Cells 9 (2009) 264.
[22] K. Xu, Y. Lam, S.S. Zhang, T.R. Jow, T.B. Curtis, J. Phys. Chem. C 111 (2007) 7411.
[23] K. Xu, J. Electrochem. Soc. 154 (2007) A162.
[24] T. Abe, H. Fukuda, Y. Iriyama, Z. Ogumi, J. Electrochem. Soc. 151 (2004) A1120.
[25] T. Abe, F. Sagane, M. Ohtsuka, Y. Iriyama, Z. Ogumi, J. Electrochem. Soc. 152 (2005) A2151.
[26] K. Xu, A. von Cresce, U. Lee, Langmuir 26 (2010) 11538.
[27] M.C. Smart, B.V. Ratnakumar, S. Surampudi, J. Electrochem. Soc. 149 (2002) A361.
[28] H.-C. Shiao, D. Chua, H. Lin, S. Slane, M. Salomon, J. Power Sources 87 (2000) 167.
[29] J.H.S.R. De Silva, R. Vazquez, P.E. Stallworth, T.B. Reddy, J.M. Lehnes, R. Guo, H. Gan, B.C. Muffoletto, S.G. Greenbaum, J. Power Sources 196 (2011) 5659.
[30] D. Aurbach, A. Zaban, Y. Ein-Eli, I. Weissman, O. Chusid, B. Markovsky, M. Levi, E. Levi, A. Schechter, E. Granot, J. Power Sources 68 (1997) 91.
[31] I.A. Courtney, J.R. Dahn, J. Electrochem. Soc. 144 (1997) 2045.
[32] B. Markovsky, M.D. Levi, D. Aurbach, Electrochim. Acta 43 (1998) 2287.
[33] C.J. Wen, R.A. Huggins, J. Electrochem. Soc. 128 (1981) 1181.
[34] C.-M. Park, J.-H. Kim, H. Kim, H.-J. Sohn, Chem. Soc. Rev. 39 (2010) 3115.
[35] L.Y. Beaulieu, T.D. hatchhard, A. Bonakdarpour, M.D. Fleiscjauer, J.R. Dahn, J. Electrochem. Soc. 150 (2003) A1457.
[36] H. Mukaibo, T. Momma, Y. Shacham-Diamand, T. Osaka, M. Kodaira, Elecotrchem. Solid-State Lett. 10 (2007) A70.
[37] T. Abe, M. Ohtsuka, F. Sagane, Y. Iriyama, Z. Ogumi, J. Electrochem. Soc. 151 (2004) A1950.
[38] P.G. Bruce, M.Y. Saïdi, J. Electroanal. Chem. 322 (1992) 93.
[39] M.D. Levi, D. Aurbach, J. Phys. Chem. B 101 (1997) 4630.
[40] M.D. Levi, D. Aurbach, J. Phys. Chem. B 108 (2004) 11693.
[41] B.A. Boukamp, Solid State Ionics 20 (1986) 159.
[42] E. Barsoukov, J. Ross Macdonald, Impedance Spectroscopy: Theory, Experiments and Applications, second edition, John Wiley & Sons, New York, 2005, p. 83.
[43] E. Peled, D. Golodnitsky, A. Ulus, V. Yufit, Electrochim. Acta 50 (2004) 391.